



OPEN

Subsea permafrost organic carbon stocks are large and of dominantly low reactivity

F. Miesner¹✉, P. P. Overduin¹, G. Grosse^{1,2}, J. Strauss¹, M. Langer^{1,3}, S. Westermann^{4,5}, T. Schneider von Deimling¹, V. Brovkin^{6,7} & S. Arndt⁸

Subsea permafrost carbon pools below the Arctic shelf seas are a major unknown in the global carbon cycle. We combine a numerical model of sedimentation and permafrost evolution with simplified carbon turnover to estimate accumulation and microbial decomposition of organic matter on the pan-Arctic shelf over the past four glacial cycles. We find that Arctic shelf permafrost is a globally important long-term carbon sink storing 2822 (1518–4982) Pg OC, double the amount stored in lowland permafrost. Although currently thawing, prior microbial decomposition and organic matter aging limit decomposition rates to less than 48 Tg OC/yr (25–85) constraining emissions due to thaw and suggesting that the large permafrost shelf carbon pool is largely insensitive to thaw. We identify an urgent need to reduce uncertainty in rates of microbial decomposition of organic matter in cold and saline subaquatic environments. Large emissions of methane more likely derive from older and deeper sources than from organic matter in thawing permafrost.

The magnitude and distribution of permafrost below the Arctic shelf seas are major unknowns for permafrost organic carbon (OC) pools¹. Sea level variations over glacial-interglacial cycles have repeatedly exposed and inundated the shelf, creating alternating terrestrial and onlapping marine strata observable in deeper sediment cores (e.g.²). Since the end of the Last Glacial Maximum (~ 21 thousand years ago, kyr) an estimated 4.7×10^6 km² of terrestrial permafrost³ has been inundated, of which approximately 2.5×10^6 km² still persists today⁴, based on numerical modelling of the thermal state of permafrost over the last four glacial cycles. The thickness of this permafrost has been constrained using industry data (e.g. boreholes^{5,6} and geophysics^{7,8}) and modelling (e.g.⁹), which show permafrost reaching more than 700 m thick below the sea floor. Since its inundation, shelf permafrost temperature has adapted to marine bottom water temperatures. Subsea permafrost and its OC pool are thus in an advanced state of warming relative to cold terrestrial permafrost^{10–12}. Subsea permafrost warms to its melting point within a few millenia after inundation¹³, but further warming requires melting of ice in the sediment and thawing can take several tens of thousands of years for permafrost a few hundred meters thick¹⁴. Although subsea permafrost is cryotic (i.e., < 0 °C), saline sediments and the downward diffusion of saline porewater from the sea floor can lower its freezing temperature, making it free of ice (i.e., cryotic but unfrozen). Modeling studies suggest that subsea permafrost is widespread below the North American Beaufort and North Siberian shelves⁴, that it has persisted for multiple glacial–interglacial cycles⁹ but its temperature and ice content, especially in deeper waters, remain uncertain¹⁵.

OC burial in the sediment of the entire Arctic shelf is estimated to be 9 Tg C/yr^{16–18}, providing a mechanism to sequester exagram-scale OC stocks over glacial cycles. Due to low temperatures and ice-rich sediments, permafrost slows microbial activity and thus preserves organic matter (OM), but the magnitude of permafrost's role has not been described or estimated. How much OC is stored in subsea permafrost is therefore very poorly constrained^{1,16,19}. A survey of experts estimates 170–740 Pg C stored in OM and 10–110 Pg C in trapped CH₄¹⁹, but estimates linked to observational data are clearly needed to constrain uncertainty. Subsea permafrost total carbon stocks below the East Siberian Sea have been estimated at 1400 Pg C²⁰ based on adding an estimated 500 Pg C in organic matter in the uppermost 25m of inundated terrestrial permafrost²¹ to 900 Pg C in greenhouse

¹Alfred Wegener Institute Helmholtz Centre for Polar and Marine Research, Potsdam, Germany. ²Institute of Geosciences, University of Potsdam, Potsdam, Germany. ³Department of Earth Sciences, Faculty of Sciences, Vrije Universiteit Amsterdam, Amsterdam, The Netherlands. ⁴Department of Geosciences, University of Oslo, Oslo, Norway. ⁵Center for Biogeochemistry in the Anthropocene, University of Oslo, Oslo, Norway. ⁶Max Planck Institute for Meteorology, Hamburg, Germany. ⁷CEN, University of Hamburg, Hamburg, Germany. ⁸BGeoSys, Department of Geosciences, Environment and Society, Université libre de Bruxelles, Brussels, Belgium. ✉email: frederieke.miesner@awi.de

gases in free and hydrate form. Similar amounts are attributed to the entire Arctic shelf area^{22,23}. The degree of decomposition of terrestrial OM derived from permafrost and deposited under marine conditions also depends on how much time it spends under oxic conditions during cross-shelf transport²⁴. Once buried deeper than a few centimeters, most shelf sediments are anoxic and decomposition slows down. OM incorporated into terrestrial permafrost and subsequently inundated by sea water is not affected by cross-shelf transport, but its microbial decomposition is affected by community composition and the sediment environment. Although permafrost thus limits OM decomposition due to low temperatures and a reduction in microbial habitat as part of the sediment pore volume is replaced by ice, the depression of the freezing point by salt permits microbial activity in cryotic sediment by preserving liquid water habitat at subzero temperatures²⁵. Lack of knowledge of permafrost distribution, temperature and soil composition has hampered quantification of the subsea permafrost OC sink's longevity and vulnerability under current and future climate conditions. The poor constraint of past and future subsea permafrost distribution augments the knowledge gap and has prevented inclusion of subsea permafrost thaw effects in Earth System Models²⁶, or in climate assessments such as SROCC or IPCC AR6^{27,28}.

Permafrost OC stocks on land are larger than current atmospheric stocks¹ and are linked to climate. Their future release is sensitive to carbon emission pathways²⁷ and creates a positive feedback loop between climate warming and one of its consequences, permafrost thaw. Subsea permafrost has already undergone a rapid warming of about 10–15 °C due to marine transgression⁴, compared to the warming of 0.2–0.4 °C per decade of continuous terrestrial permafrost²⁹ in the early 21st century. Subsea permafrost warming and thaw is therefore expected to be further advanced than for terrestrial permafrost. This post-transgression warming may have created pathways for gas flow, particularly through ebullition, or have destabilized gas hydrates. Both have been invoked to explain observations of greenhouse gas release from the Arctic seabed³⁰, although the source of gas remains controversial^{31–34}. Field studies of carbon sources^{35,36}, studies of frozen sediment^{4,37}, and constraints on permafrost distribution^{4,7,38} have not led to consensus on current methane flux emissions and sources nor to an understanding of their relationship to permafrost or its thawing. There remains therefore an urgent need to better estimate OC and greenhouse gas pools associated with subsea permafrost below the Arctic shelf. In this study, we estimate the accumulation of OC in subsea permafrost and its decomposition over four glacial cycles in order to estimate modern OC stocks and to constrain potential greenhouse gas emissions due to the decomposition of this OC as permafrost thaws.

We used model results of the thermal state and the liquid pore water fraction of the subsurface over the last 450 kyr⁴ and conceptualized microbial decomposition of buried OM as a function of the liquid water habitat in the sediment. Our modeling shows that subsea permafrost has accumulated around 2800 Pg OC over the past 450 kyr, until pre-industrial time. This is approximately 2 times the estimated terrestrial permafrost region OC stock (1460–1600 Pg OC, including unfrozen deposits in that region^{39–44}), although the area underlain by subsea permafrost is approximately only 18% of its terrestrial counterpart⁴⁵. Our model results are based on all sediment deposited within the model time—up to 150 m below sea floor—while the estimate for the terrestrial OC stock is restricted to only the uppermost 50 m, independent of deposition period. Comparing the same depth intervals as a proxy for deposition period underscores the larger OC reserve on the shelf: 90% of the OC stock in subsea permafrost is located in the upper 50 m below sea floor of the sediment column (Supplementary Table S2). The persistent presence of permafrost on the Arctic shelves over the past up to 2 Myr⁹ is thus likely to have preserved more OC than is currently estimated to be stored in permafrost on land, forming a substantial long-term sink for terrestrial carbon in the Earth System.

Our work thus shows that a vast pool of OC has been accumulating beneath the Arctic Shelf over multiple glacial cycles. The reactivity of this remaining OC and the degree of its preservation from aging by permafrost, play a decisive role in determining potential emissions from microbial decomposition when it thaws. However, our model also shows that, since this OC pool is mostly aged and has been subject to decomposition, what remains is not very reactive. We model current permafrost OC decomposition rates to be 1.4 Tg C/yr (0.8–2.1) within sediments deposited over the past 450 kyr. Accelerated permafrost thaw will increase these rates, but with an upper bound of 48 Tg C/yr (25–85) based on Arctic shelf depositional history, placing an upper bound on potential emissions. We conclude that subsea permafrost OC is largely insensitive to thaw, but that a better understanding and quantification of its preservation with field data would help constrain risks associated with this first modeled estimate. The implication is that decomposition products, i.e. greenhouse gases, have been sequestered within and/or below permafrost (the former due to upward thaw at the permafrost base) in some form, or were emitted from the seabed. To better constrain climate risks associated with emissions from gas hydrate dissociation and/or greenhouse gas emissions, our understanding of subsea permafrost thaw, its overlap with gas hydrates and the microbial control on emissions of carbon dioxide vs. methane must be improved.

Results

Organic carbon accumulation below the Arctic shelf. Buried OC is calculated in our model from spatially uniform net mass accumulation rates of terrestrial and marine material⁴ with assigned OC contents based on medians of observational data for marine and terrestrial sediments (Table 1). Sediment OC content before 450 kyr before present (BP) was ignored, i.e. we considered only OC accumulated within our modeled time period. With this simplified approach, we estimated that 3600 Pg C was buried beneath the seabed over the past 450 kyr for the portion of the Arctic Shelf region currently underlain by permafrost (Fig. 1a). However, both accumulation rates and OC contents vary greatly in space and time in response to glacial and deglacial cycles, with associated changes to drainage of watersheds and glacial isostatic adjustment, and in response to sea level changes. Recent work shows that deglaciations can amplify permafrost carbon release, primarily by mobilizing organic-rich surficial deposits which are then transported to the sea^{46–49}. This carbon may partially correspond to sediments of today's Yedoma region, which currently covers 2.6×10^6 km² of Siberia⁵⁰ and presumably

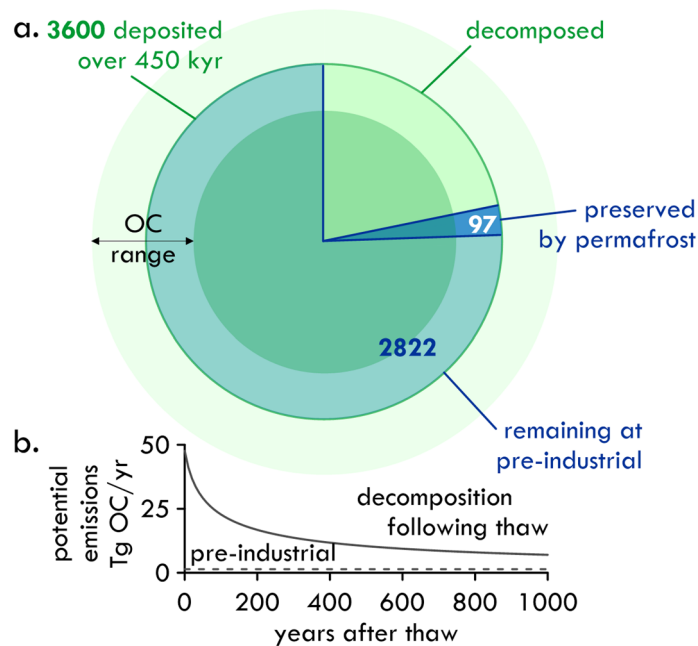


Figure 1. (a) Organic carbon stocks in subsea permafrost at pre-industrial time and potential emissions. In our model 3600 Pg C are buried on the Arctic shelf over the past 450 kyr (green circle). The radial range stems from plausible variability of OC deposition rates (Table 1). This carbon decomposes slowly over time, leaving 2822 Pg C remaining at pre-industrial time. Permafrost plays a small role in OC quantity—only 97 Pg C of these 2822 Pg C are preserved because of permafrost (blue slice), since slow decomposition occurs even under cryotic conditions. (b) When thawed, OM decomposition rates increase 30-fold from about 1.4 Tg C/yr (at pre-industrial time for all sediment deposited over the model period) to over 47 Tg C/yr, and drop over 1000 years to 7 Tg C/yr (lower graph). Realistic thaw rates for subsea permafrost, however, lie below 5 cm/yr over this period^{10,26} and constrain decomposition rates to below this latter value.

Stratigraphy	Sedimentation	OC contents		
	Rates	1st quartile	Median	3rd quartile
Marine	30 cm/kyr (0.3 mm/a)	0.57 wt%	0.99 wt%	1.43 wt%
Terrestrial	10 cm/kyr (0.1 mm/a)	1.02 wt%	1.90 wt%	3.40 wt%

Table 1. Stratigraphy divisions and their OC contents. Sedimentation rates are assumed as in⁴. OC contents are taken from^{43,53,60}. Quartiles are defined using the distribution of observations shown in Supplementary Fig. S1a,b.

extended far northward of the modern coastline^{9,51}. To estimate the effect of variability in OC deposition, we applied 25–75% quantiles of the OC contents in fresh material for both marine and terrestrial sedimentation, generating burial of an OC range: 1960–6140 Pg C (Fig. 1a).

Previous estimates of recent OC deposition are 10 Tg C/yr for the Russian Arctic shelf (2.15 g C/m²/yr)¹⁸ and 8.7 Tg C/yr for the entire Arctic shelf (1.73 g C/m²/yr)¹⁷ and are of the same order of magnitude as our mean modelled OC deposition rate: 8 Tg C/yr (4.4–13.6) for the past 450 kyr over the entire modelled region and 11.9 Tg C/yr (6.8–17.2) at pre-industrial time for the subsea permafrost region. Current estimates of terrestrial OC sedimentation rates on the Arctic shelf range from 1.8 Tg OC/yr to 13 Tg OC/yr (means for shelf seas: minimum, Beaufort, to maximum, East Siberian)⁵² based on sediment OC contents and Pb-dating of sediments for accumulation rates, for a total of 45 Tg OC/yr for the entire Arctic Shelf. The burial efficiency is estimated at around 10%¹⁸, which would imply accumulation of around 4 Tg OC/yr, but this estimate excludes marine derived OC. As a function of sediment depth, our OC contents (1.16 wt% ± 0.75) fall within the range of observed values from shelf boreholes (mean 1.06 wt% ± 1.05, Supplementary Fig. S1c,d^{53–56}). Our sedimentation scheme thus generates initial shelf OC stocks that correspond to observationally based estimates of burial rates.

Decomposition of organic matter in subsea permafrost. We calculated OM decomposition rates with a reactivity continuum model (RCM) (Refs. ^{57,58}, “Methods” section), exploring subsea permafrost OC evolution for a plausible range of reactivity parameters. We chose different parameter sets for marine and terrestrial

deposits based on measurements^{58,59} and the inversion of observed incubations from the Siberian Shelf³⁷. Output from our thermal model included sediment temperature and its liquid water and ice contents⁴, so that both temperature and the available volume of microbial habitat could be used as limiting factors for microbial activity.

To address uncertainties in decomposition response to temperature, we performed two simulations. In the first simulation, we only relate decomposition to the availability of liquid water in the sediment pore space, regardless of sediment temperature (Eq. (5), “Methods” section). In this case, slow decomposition occurs even under cryotic conditions and OC stocks of approximately 2822 Pg C (1518–4982, for quartiles of initial OC content) remained at pre-industrial time (Supplementary Table S1), i.e. approximately 22% (19–29) of the deposited OM had decomposed over the 450 kyr period (Fig. 1a).

In the second, more conservative reactivity simulation, in which decomposition was halted completely in cryotic sediment (Eq. 4, “Methods” section), 3252 Pg C (1762–5633) remained and only 10% (8–10) of the deposited OM had decomposed.

We found the highest amounts of OC ($> 30 \text{ kg m}^{-3}$) in the regions that spent the most time under subaerial conditions, i.e., in coastal and never-glaciated regions, which results in total column OC accumulations of up to 1400 kg m^{-2} over the last 450 kyr in central and near-shore shelf areas (Fig. 2). These regions had the highest proportion of terrestrial sediment, which contained more OC than marine-dominated sediments further out on the shelf (Table 1), and had deeper and colder subsea permafrost⁴, so that OM decomposed more slowly than further offshore.

Preservation of organic matter by subsea permafrost. To assess the impact that permafrost has on OM preservation we compared our OC accumulation results to a scenario in which we allowed decomposition to occur independently of temperature, equivalent to a permafrost-free shelf scenario (Supplementary Table S1). The percentage of post-industrial permafrost OC that results solely from the presence of permafrost over the last 450 kyr is a measure for the permafrost preservation effect.

We found that only marginally more OC is stored with permafrost (2822 PgC) than without (2725 PgC), a preservation effect of 3% (Fig. 3). For the case in which decomposition occurs whenever sediment is above 0°C , the preservation effect is higher at 16%. Magnitudes of preservation reached a maximum of around 60 Tg km^{-2} but were spatially variable (Fig. 3). Applying terrestrial-fit reactivity parameters to the whole sediment column, the preservation effect is even lower ($< 1.2\%$). Higher reactivity parameters, corresponding to marine OC reactivity, result in a preservation effect of 48%, i.e. permafrost almost doubles OC storage when reactivity is high but has little effect when the OC is difficult to decompose (Supplementary Table S1). As a result, permafrost typically preserves a smaller fraction of OC close to the present-day coast (where terrestrial sediment dominates) than it does midshelf, particularly below the broad shelves of the East Siberian Sea (Fig. 3). In areas with high marine fraction in the sediment column, locally up to 7% of the OC remaining after 450 kyr was preserved by the presence of permafrost on the largely unglaciated shelves of the eastern Kara, the Laptev, the East Siberian and the Chukchi seas.

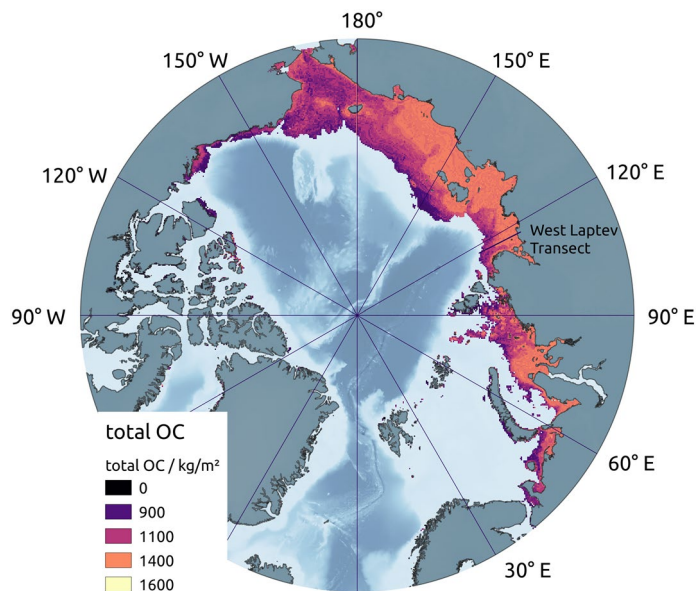


Figure 2. Total organic carbon content within subsea permafrost at pre-industrial time. The map shows the total amount of OC, summed over the sediment that accumulated within the last 450 kyr. OM decomposition was permitted in the liquid water volume of the sediment column, even at cryotic temperatures, with median terrestrial and marine sediment OC burial rates and OM reactivity parameters of $a = 50 \text{ yr}$ and $\nu = 0.15$ for marine and $a = 0.25 \text{ yr}$ and $\nu = 0.003$ for terrestrial deposits. Locations where subsea permafrost was not present at pre-industrial time are excluded.

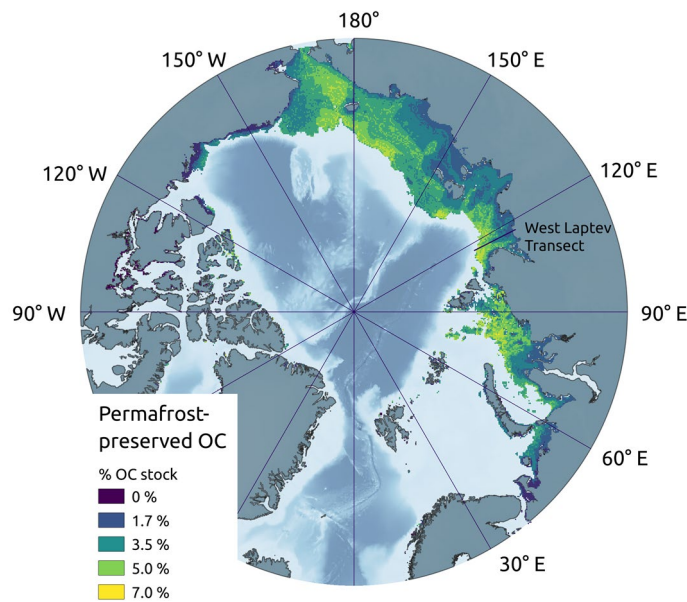


Figure 3. Percentage of organic carbon content that was preserved by the presence of permafrost during the last 450 kyr in the region underlain by subsea permafrost at pre-industrial time. The color scale indicates the percentage of pre-industrial OC stock (Fig. 2) preserved by permafrost (i.e. % OC exceeding OC accumulation in the absence of permafrost).

These patterns of how OM preservation varies with sediment and OM reactivity are illustrated in Fig. 4. The total OC content at pre-industrial time is shown for a north-south depth profile with approx. 600 m thick permafrost at the coastline of the western Laptev Sea (Ref.⁴, transect location indicated in Figs. 2, 3), where large differences in the OC content can be observed between the different layers of sediment: as a result of both higher reactivity and higher liquid water content at temperatures below 0 °C, more OC is stored in non-saline terrestrial sediment layers than in saline onlapping transgressive sediments (Fig. 4c).

Decomposition rates after thaw. To assess the effects of present and future permafrost thaw, we additionally modelled the OM decomposition rates beginning from pre-industrial time (1850CE) until 3000CE, permitting OM to age regardless of temperature or ice content. This is equivalent to permitting OM reactivity to vary as it would in the absence of permafrost, in either a cryotic (≤ 0 °C) or thawed (unfrozen) sediment, respectively. It simulates the instantaneous thaw at 1850CE of sediment and OM that had been deposited over the 450 kyr before pre-industrial time and is therefore an upper bound on greenhouse gas production due to thaw of modern subsea permafrost.

Within the subsea permafrost sediment volume beneath the entire Arctic shelf, this instant thawing increased OC decomposition rates from 1.4 Tg OC/yr (0.8–2.1 Tg OC/yr) at the end of our model time to 48 Tg OC/yr (25–85 Tg OC/yr), a 34-fold increase. Rates of subsea permafrost thaw are, however, low, since mean annual seabed temperatures for much of the Arctic shelf are negative⁶¹. Inferred subsea permafrost thaw rates range from tens of cm/yr following transgression to less than a cm/yr after a millennium of warming beneath the seabed¹⁰. Modelled thaw of subsea permafrost under future warming scenarios ranges from 1–5 cm/yr over the period from today until 3000CE²⁶, the latter under the high-emission SSP 8.5 scenario²⁷. Earth system modeling suggests that future thaw of subsea permafrost can be directly linked to a reduction of sea ice cover²⁶, but that complete thaw of subsea permafrost is unlikely to occur by 3000CE. Rates of OC decomposition are thus likely to be at least three orders of magnitude lower than our upper bound of 48 Tg OC/yr. Even in the case of complete thaw of the sediment deposited in our model runs, prior decomposition of the OM will have decreased decomposition rates by more than a factor of 6 after 1000 yr, to less than 8 Tg C/yr (Fig. 1b).

Discussion

Although our model generates a globally significant pre-industrial OC pool beneath the Arctic Shelf, it probably underestimates this pool for a number of reasons. Firstly, our estimate of Arctic shelf OC stocks does not include OC decomposition products that may be stabilized or trapped by permafrost (e.g., gas hydrates³⁸). Since gas diffusivity in frozen permafrost is orders of magnitude lower than in unfrozen sediment, ice-bearing permafrost slows or effectively halts gas diffusion⁶². Permafrost can thus prevent upward greenhouse gas migration, capping gaseous C stocks and delaying their re-introduction into the global carbon cycle⁶³.

Gas hydrates within or below permafrost (permafrost-associated) may derive from underlying reservoirs, which produce thermogenic gas that migrates to shallower depths, where it may integrate into permafrost and is stabilized by lower temperatures⁶⁴. Estimates for the amount of gas hydrates associated with permafrost in the Arctic range from around 1% of global gas hydrates (20 Pg)³⁸ to estimates that suggest up to 800 Pg of

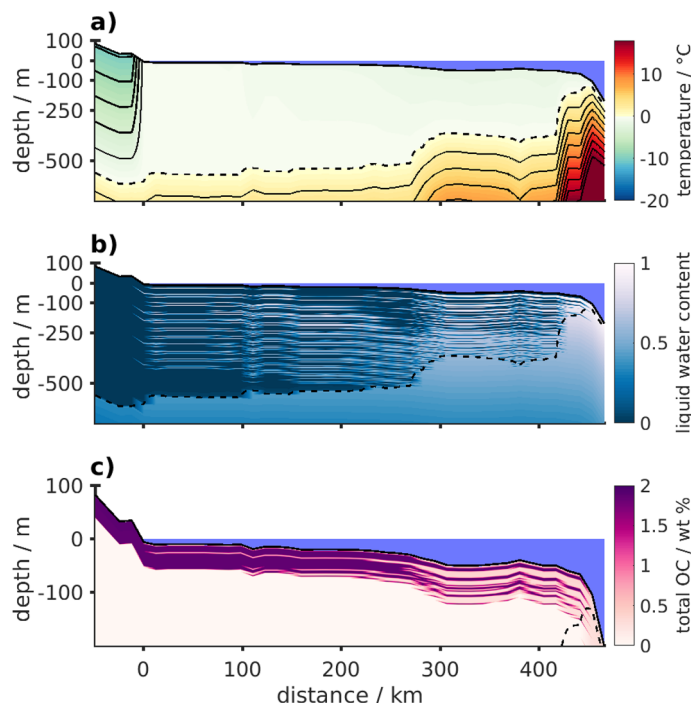


Figure 4. Organic carbon degradation illustrated on a south-north transect in the western Laptev Sea. Sediment temperature (a), liquid water content in the pore space (b), and organic carbon content (c) stored along a south-north transect (from left to right) in the western Laptev Sea (along 117° E) at pre-industrial time. Panel (c) shows sediment organic carbon (OC in wt%) for decomposition scaled to liquid water content. OM was only accumulated within the last 450 kyr with median terrestrial and marine sediment OC burial rates and decomposition was scaled with reactivity parameters of $a = 50$ yr and $\nu = 0.15$ for marine and $a = 0.25$ yr and $\nu = 0.003$ for terrestrial deposits. The location of this transect in the western Laptev Sea is shown in Figs. 2, 3. Note the different depth scales between panels (a)/(b) and panel (c).

methane may have accumulated below and within permafrost in the period of one glacial cycle³¹. Inclusion of gas hydrates in thermal properties of the permafrost would improve the model but would be spurious given our poor knowledge of gas hydrate distribution for most of the Arctic shelf. The presence of gas hydrates lowers the thermal conductivity of the permafrost sediments⁶⁵. Its latent heat of formation or dissolution can similarly increase heat transfer requirements⁶⁶ increasing thermal inertia. Gas hydrate dissolution, usually via pressure changes associated with thaw from above or via geothermal warming, can change the pore space morphology of the sediment and freshen pore space fluid⁶⁷, raising its freezing point. Because the gas hydrate stability zone is different from the stability field of liquid water, permafrost-associated gas hydrates can exist at depths that overlap (intraparfrost) and extend below (subpermafrost) permafrost. Understanding where gas hydrates reside in the sediments is therefore an important factor to fully account for thermal dynamics in future submarine permafrost development.

Groundwater flow and associated changes in sediment salinity can also lead to changes in permafrost distribution, for example through thaw⁶⁸ or an increase in its extent⁶⁹. Analogous to gas hydrates, our ignorance of ground water flow makes its inclusion in thermal modeling speculative. The effect of including ground water would change permafrost distribution but have little effect on sediment OM decomposition for the reasons described above; it would increase OC stocks and potential emissions without recourse to OM decomposition. Finally, OM decomposition may be inhibited by end product accumulation, including CO₂ and CH₄, which are confined almost everywhere by low gas diffusivity of the frozen sediment, and by the low solubility of saline porewater solutions.

A second factor that probably renders our estimate of the subsea permafrost OC pool too low is the choice of moderate parameters for the reactive continuum model of decomposition. Although the chemical composition of OM has traditionally been regarded as exerting the dominant control on its reactivity, recent studies support the notion of apparent OM reactivity as a dynamic ecosystem property (e.g.^{70–73}). In this case, reactivity is controlled by the chemical composition of the OM, and also by a complex and dynamic interplay with environmental variables such as temperature, microbial community structure and abundance, bio-energetics, enzyme kinetics or protection by mineral surfaces^{74–76}. The parameters of OM decomposition models implicitly account for these controls and, thus, vary widely across different environments^{58,59}. We used two sets of values for transgressive and regressive sediment layers over the whole model area and time based on a compilation of inversely determined values from measurements and incubation experiments (see “Methods” section). The comparably high apparent reactivity of marine OM leads to faster decomposition than the lower apparent reactivity of OM stored

in terrestrial deposits, where we see a high initial apparent reactivity followed by a near stop in decomposition. Using the marine OM reactivity parameters for the whole sediment column resulted in an overall smaller OC pool (1985 Pg C), but with greater permafrost preservation effect (933 Pg C).

Methods

Permafrost model. The thermal state of the subsurface was estimated with a 1D numerical model [Cryogrid2⁷⁷] solving the heat equation over a $7000 \times 7000 \text{ km}^2$ grid⁴ of 12.5 km spacing. Sedimentation and permafrost dynamics were modelled over the last four glacial cycles (last 450 kyr) on the Arctic shelf between -120 and 18 m above modern sea level, an area of approximately $4.5 \times 10^6 \text{ km}^2$ and therefore roughly twice the area of modern subsea permafrost⁴. The thickness of sedimentary deposits was taken from the GlobSed database⁷⁸, below which bedrock was modelled. For each grid cell the model produced sediment temperature, porewater salinity, and volumetric ice and liquid water contents within 2 km below the seafloor or land surface at 2 m discretization over the last 450 kyr.

The model run was initialized with the steady state solution between the local geothermal heat flux interpolated from the global database of⁷⁹ and the surface condition at 450 kyr BP for all modelled locations. We synthesized the dynamic surface forcing condition from sea level history, glaciation and time series of mean annual air temperature over the last 450 kyr using the sea level curve from⁸⁰, and glacial ice cover extent and thickness and surface air temperature simulated by the intermediate complexity Earth System Model CLIMBER-2^{81,82}.

Organic carbon in shelf sediments. Organic carbon contents of sediment and linear net sedimentation rates were set for terrestrial and marine deposition for the circumarctic model region. To initialize the OC pool of subsea permafrost, we linked estimated OC contents to the modelled sediment stratigraphy. Available observations of total organic carbon contents for terrestrial Weichselian deposits and for Arctic shelf marine sediments are shown in Supplementary Fig. S1a–c. Observed sediment OC contents span a wide range of values. To reflect this variability as a source of uncertainty in our model, we also calculated stocks for the first and third quartile OC contents based on these observational data sets.

We modelled deposition over the last 450 kyr at the linear net sedimentation rates chosen in Table 1, resulting in deposition of 45–135 m of the upper sediment column. For these sediment layers, OC decomposition began at the time of deposition with initial contents of fresh organic matter depending on the depositional milieu (i.e. regressive/transgressive). For deeper (i.e. older than 450 kyr) material, the carbon content was initialized as zero, equivalent to the absence of any OC in deeper sediment strata (Fig. 5).

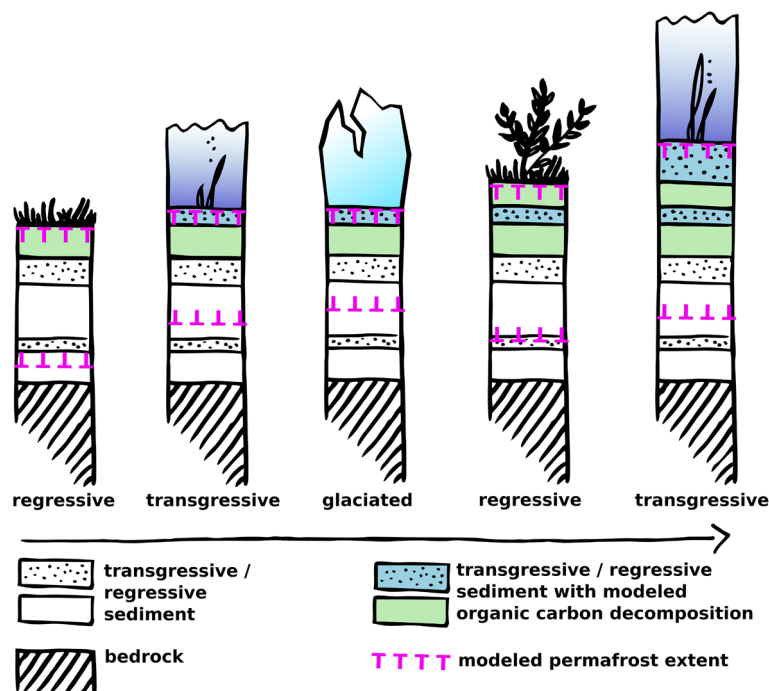


Figure 5. Modeling of sedimentation and heat flow during regressive (first and fourth column), transgressive (second and last column) and glaciated (third column) periods produced a simplified sediment stratigraphy and permafrost extent below the sea floor (dashed magenta lines) over depth. Sedimentation, OM contents and decomposition rates were modelled for the Arctic shelf for the past 450 kyr (time arrow). OC stocks are reported for sediment that accumulated over this period (colored strata).

Organic matter decomposition. OC content over time was estimated based on time elapsed since deposition and on the sediment's physical state. To calculate the OC content of sediment buried for time t , where $t = 0$ is the time of sedimentation, we employed the reactive continuum model^{57,58} for organic decomposition

$$\text{OC}(t) = \text{OC}_0 \left(\frac{a}{a+t} \right)^{\nu}, \quad (1)$$

with initial values OC_0 based on Table 1.

As a first-order estimate, we used a *decomposition time* τ in Eq. (1), that disregards time periods where the sediment's temperature is below 0 °C, preserving OC reactivity until positive temperatures are restored. With the indicator function

$$\chi(t) = \begin{cases} 0 & T(t) < 0^{\circ}\text{C} \\ 1 & T(t) \geq 0^{\circ}\text{C} \end{cases}, \quad (2)$$

we defined the decomposition period as

$$\tau(t) = \int_0^t \chi(s) ds \quad (3)$$

and Eq. (1) becomes

$$\text{OC}(t) = \text{OC}_0 \left(\frac{a}{a+\tau(t)} \right)^{\nu}. \quad (4)$$

In saline marine sediments, the 0 °C isotherm and the frozen/unfrozen interface are usually not coincident due to freezing point depression of the brine in the pore water. We therefore additionally linked the microbial activity to liquid water content rather than to temperature alone. Assuming that microbial activity is limited to the volume of sediment liquid water content θ , we adjusted the decomposition period by the volume fraction of liquid water to

$$\tau(t) = \int_0^t \frac{\theta(s)}{\eta} ds, \quad (5)$$

where η is the porosity. The fraction $\frac{\theta(s)}{\eta}$ yields a value between zero and one. The effective decomposition time was therefore linearly scaled to the available liquid water habitat in the sediment. This ignores the effects of differences in temperature or salinity on reactivity, equivalent to the assumption that OM decomposition is primarily dependent on habitat availability, and that halocryophilic communities are adapted to a range of environmental conditions. We understand that this introduces currently unquantifiable uncertainties.

RCM parameterization. The reactivity parameters a and ν of the RCM are essentially free, positive parameters that completely determine the shape of the initial, continuous distribution of OM compounds over the reactivity spectrum and, thus, the apparent reactivity of OM and its evolution during burial in the sediment⁵⁷. In general, low a and high ν values indicate a dominance of more reactive compounds and thus result in a higher apparent OM reactivity, while high a and low ν values indicate the dominance of less reactive compounds and a low reactivity⁵⁸. In addition, the value of a also controls the lifetime of the most reactive compounds and determines the decrease of OM reactivity with burial time/depth. It is often considered as an indicator for the “freshness” or “initial age” of the deposited OM^{57,83}. The shaping parameters of the RCM may be inverted from incubation experiments or estimated from borehole OC records with sufficiently good age control^{58,59}. Low a values result in a higher initial OM reactivity (for the same ν) and a rapid decrease in this reactivity with OM age, while high a values lead to a lower initial reactivity but a slower decrease in reactivity with age (Ref.⁵⁸, Supplementary Fig. S2). A compilation of previously published, inversely determined parameter values for marine sediments reveals that the global-scale variability in benthic OM reactivity is mainly driven by the large variability in parameter a . The wide range of values spans a very wide range of conditions from fresh pure marine diatom OC degrading in the lab to pre-degraded OC from marine sediments typically found on the continental slope. Published values vary from $a = 3.1e^{-4}$ yr for highly reactive, fresh phytoplankton material that was decomposed under laboratory conditions to $a = 1.4e^5$ yr for OM deposited in the Central Equatorial Pacific^{57,84}. The typical value range for OC found in coastal marine sediments, however, is $a \approx 5$ to 70 yr^{58,59,85}. In contrast, reported ν parameter values for marine sediment mostly fall within the range $0.1 < \nu < 0.2$ ^{57–59}, thus indicating that ν remains relatively constant across largely different depositional environments. This finding is also fully consistent with the empirically derived power law description of OM decomposition⁸³ that applies a globally constant parameter. Based on these findings, we chose $a = 50$ yr and $\nu = 0.15$ ^{58,59} for the marine sediment layers in our stratigraphy.

Values of a and ν for terrestrial layers were inversely determined by fitting the RCM to reported CO₂ production rates during anoxic incubations of permafrost samples at 4 °C reported by³⁷, which are, to our knowledge, the only values available for subsea permafrost sediment OC. Best fit (a, ν) couples are found by solving the least squares minimization problem:

$$\min_{a,v} \sum_{i=1}^n \left(\frac{v}{a+t} G_0 \left(\frac{a}{a+t} \right)^2 - R_{i,obs} \right)^2,$$

where $R_{i,obs}$ are the measurements, G_0 the initial OM content and t denotes the incubation time. This results in values of $a = 0.0007$ yr ($1e^{-8}-2e^{-3}$) and $v = 0.005$ ($4e^{-4}-2e^{-3}$). We chose $a = 0.25$ yr and $v = 0.003$ for terrestrial sediment layers. Choosing a lower than 1 yr and a comparably low v is fully consistent with three-pool model based on a circumpolar database for terrestrial OC that shows widely observed slow and continuous decrease in OC reactivity over time⁸⁶.

Sources of uncertainty. Sources of uncertainty in the reported OC stock estimates are the OC content of buried terrestrial and marine sediment on the shelf and the choice of RCM reactivity parameters a and v . Shelf deposits are more difficult to characterize than terrestrial, where surficial geomorphology, remote sensing and denser sampling can be used to characterize the distribution of OC stocks. Observation of shelf sediment, particularly by sampling in the shallow waters (< 20 m) of much of the Siberian shelf, has been limited by ice cover and restricted access to shallow-draught ships. For this reason, upscaling of local observations and propagation of observation-based uncertainties, as for OC stock estimation on land³⁹, are not possible. Our OC contents are, however, based on databases of observed values of buried terrestrial Late Pleistocene and marine sediment OC^{44,53,60}, which are applied uniformly over the Arctic shelf depending on whether the shelf is exposed during transgressions or inundated during regressions, respectively, to create site specific sediment stratigraphy. Variability in OC content (see Supplementary Fig. S1a,b) is characterized using the first and third quartiles (Q1, Q3) of the distributions. This approach ignores spatial and temporal heterogeneity in sedimentation and erosion but brackets results of simulations, for which we report resulting OC stocks resulting from *median* (Q1–Q3) OC contents. Holocene sediments with higher OC contents, including thermokarst lake and alas deposits⁸⁷, peatlands⁴⁰ or the Yedoma complex deposits⁴⁴ are generally eroded during coastline retreat driven by thermo-erosion and sea level rise along the Arctic coastline. The OM released by erosion is subsequently transported out of the shelf region (for example, by ice-rafting), subject to turnover in the water column, or deposited on the seabed, where it undergoes turnover prior to burial. Available buried OC contents on the Arctic shelf for samples of millennial to glacial cycle time-scale sediment records have lower median values than either the marine sediment or terrestrial permafrost data we use as input (Supplementary Fig. S1c,d).

Our somewhat arbitrary choice of the poorly constrained RCM parameter a introduces further uncertainty, and reflects a true uncertainty in our understanding of subsea permafrost OM decomposition. Low terrestrial OM reactivity make changes to parameterized reactivity negligible in terms of their impact on remaining OC stocks over long time periods. Changing a in sediment of terrestrial origin from our value of 0.25 to 0.0007 (from³⁷), while holding other parameters equal, reduces estimated OC stocks by around 2% (from 2822 to 2778 Pg OC). Changing a for marine OM can affect remaining stock more dramatically, but the OC content of marine sediment can dampen the effect on total estimates. Decreasing (increasing) marine a while holding other parameters constant from 50 to 5 yr (500 yr) changes the total subsea permafrost OC stock estimate from 2822 to 2710 Pg OC (2980 yr), a reduction (increase) of 4% (6%), respectively.

Most incubation experiments of microbial activity in permafrost are conducted at 4–20 °C. Subsea permafrost is mostly between –2 and 0 °C where temperature variations are not as pronounced as changes in the ice content. We therefore lack data to properly parameterize the dependence of OM reactivity on temperature for subsea permafrost; however, the inversely determined parameter fits implicitly account for temperature. To account for uncertainties in our assumed parameterization, (a, v) couples for marine and terrestrial sediment OC were also applied to the whole sediment column for a high and a low reactivity scenario, respectively.

Two general points can be made about the uncertainties calculated as described. Firstly, uncertainty in OC stocks that results from changes to the estimates of OC content in sediment are greater than uncertainty resulting from assumptions regarding OC reactivity. The choice of different RCM parameter couples (a, v) results in a smaller range in the estimated OC pool, than changing the initial OC content. As an example, our most plausible estimate for remaining OC stocks, 2822 Pg OC has associated uncertainty ranges of (1518–4982) due to OC sediment content uncertainty but only (1985–3497) when making the assumption that ALL sediment is of marine or terrestrial origin in terms of its reactivity (combined, the two effects result in a range of 2822 Pg OC (1075–5963)). This suggests that constraining subsea permafrost OC stocks is more effectively done by better describing sedimentation composition than by improving our estimates of OC reactivity. Secondly, given the glacial cycle time scale for degradation, the form of the RCM itself imposes limits on the degree of decomposition that can be attained or avoided. For example, even lower a values will make almost no change to resulting OC stocks, since they imply such a low reactivity that much longer time scales would be required to change OC stocks appreciably.

Data availability

Input data for modelling is available from the sources listed. Output data for the permafrost map is available⁸⁸.

Code availability

Program code is based on CryoGrid, as described in⁴. A community version of this code is available at (<https://github.com/CryoGrid/CryoGrid>). The specific code for this experiment is available from the authors per request.

Received: 14 December 2022; Accepted: 4 June 2023

Published online: 09 June 2023

References

1. Schuur, E. A. G. *et al.* Climate change and the permafrost carbon feedback. *Nature* **520**, 171–179 (2015).
2. Rachold, V. *et al.* Nearshore arctic subsea permafrost in transition. *EOS Trans. Am. Geophys. Union* **88**, 149–150 (2007).
3. Lindgren, A., Hugelius, G., Kuhry, P., Christensen, T. R. & Vandenbergh, J. GIS-based maps and area estimates of northern hemisphere permafrost extent during the last glacial maximum. *Permafrost Periglac. Process.* **27**, 6–16 (2016).
4. Overduin, P. *et al.* Submarine permafrost map in the arctic modelled using 1D transient heat flux (SuPerMAP). *J. Geophys. Res. Oceans* **124**, 3490 (2019).
5. Hu, K., Issler, D. R., Chen, Z. & Brent, T. A. Permafrost investigation by well logs, and seismic velocity and repeated shallow temperature surveys, Beaufort–Mackenzie Basin. *Geol. Surv. Canada Open File* **6956**, 33 (2013).
6. Ruppel, C. D., Herman, B. M., Brothers, L. L. & Hart, P. E. Subsea ice-bearing permafrost on the U.S. Beaufort margin: 2. Borehole constraints. *Geochem. Geophys. Geosyst.* **17**, 4333–4353 (2016).
7. Brothers, L. L., Herman, B. M., Hart, P. E. & Ruppel, C. D. Subsea ice-bearing permafrost on the US Beaufort margin: 1. Minimum seaward extent defined from multichannel seismic reflection data. *Geochem. Geophys. Geosyst.* **17**, 4354–4365 (2016).
8. Portnov, A. *et al.* Offshore permafrost decay and massive seabed methane escape in water depths > 20 m at the South Kara Sea shelf. *Geophys. Res. Lett.* **40**, 3962–3967 (2013).
9. Romanovskii, N. N., Hubberten, H. W., Gavrillov, A. V., Tumskey, V. E. & Kholodov, A. L. Permafrost of the East Siberian Arctic shelf and coastal lowlands. *Quat. Sci. Rev.* **23**, 1359 (2004).
10. Angelopoulos, M., Overduin, P. P., Miesner, F., Grigoriev, M. N. & Vasiliev, A. A. Recent advances in the study of Arctic submarine permafrost. *Permafrost Periglac. Process.* **31**, 442–453 (2020).
11. Junker, R., Grigoriev, M. N. & Kaul, N. Non-contact infrared temperature measurements in dry permafrost boreholes. *J. Geophys. Res.* **113**, B04102 (2008).
12. Shakhova, N. *et al.* Ebullition and storm-induced methane release from the East Siberian Arctic Shelf. *Nat. Geosci.* **7**, 64–70 (2013).
13. Malakhova, V. V. & Eliseev, A. V. The role of heat transfer time scale in the evolution of the subsea permafrost and associated methane hydrates stability zone during glacial cycles. *Glob. Planet. Change* **157**, 18 (2017).
14. Lachenbruch, A. H. Thermal effects of the ocean on permafrost. *Bull. Geol. Soc. Am.* **68**, 1515 (1957).
15. Malakhova, V. V. & Eliseev, A. V. Uncertainty in temperature and sea level datasets for the Pleistocene glacial cycles: Implications for thermal state of the subsea sediments. *Glob. Planet. Change* **192**, 103249 (2020).
16. McGuire, A. D. Sensitivity of the carbon cycle in the Arctic to climate change. *Ecol. Monogr.* **79**, 523–555 (2009).
17. Stein, R. & Macdonald, R. W. *The Organic Carbon Cycle in the Arctic Ocean* 315–322 (Springer, 2004).
18. Vetrov, A. A. & Romankevich, E. A. *Carbon Cycle in the Russian Arctic Seas* 331 (Springer, 2004).
19. Sayedi, S. S. *et al.* Subsea permafrost carbon stocks and climate change sensitivity estimated by expert assessment. *Environ. Res. Lett.* **15**, 124075 (2020).
20. Shakhova, N. *et al.* Geochemical and geophysical evidence of methane release over the East Siberian Arctic Shelf. *J. Geophys. Res. Oceans* **115**, C8 (2010).
21. Zimov, S. A., Schuur, E. A. G. & Chapin, F. S. Permafrost and the global carbon budget. *Science* **312**, 1612–1613 (2006).
22. Chen, M. *et al.* Subsea permafrost as a potential major source of dissolved organic matter to the East Siberian Arctic Shelf. *Sci. Total Environ.* **777**, 146100 (2021).
23. Vonk, J. E. *et al.* Activation of old carbon by erosion of coastal and subsea permafrost in Arctic Siberia. *Nature* **489**, 137 (2012).
24. Bröder, L. *et al.* Historical records of organic matter supply and degradation status in the East Siberian Sea. *Org. Geochem.* **91**, 16–30 (2016).
25. Elberling, B. & Brandt, K. K. Uncoupling of microbial CO₂ production and release in frozen soil and its implications for field studies of arctic C cycling. *Soil Biol. Biochem.* **35**, 263–272 (2003).
26. Wilkenskeld, S., Miesner, F., Overduin, P. P., Puglini, M. & Brovkin, V. Strong Increase of Thawing of Subsea Permafrost in the 22nd Century Caused by Anthropogenic Climate Change. *The Cryosphere* **16**, 1057–1069 (2022).
27. Canadell, J. *et al.* Climate change 2021: The physical science basis. In *Contribution of Working Group I to the Sixth Assessment Report of the Intergovernmental Panel on Climate Change* (eds Masson-Delmotte, V. *et al.*) (Cambridge University Press, 2021).
28. Meredith, M. *et al.* IPCC Special Report on the Ocean and Cryosphere in a Changing Climate 203–320 (Cambridge University Press, 2019).
29. Biskaborn, B. K. *et al.* Permafrost is warming at a global scale. *Nat. Commun.* **10**, 264 (2019).
30. Shakhova, N. *et al.* Extensive methane venting to the atmosphere from sediments of the East Siberian Arctic Shelf. *Science* **327**, 1246–1250 (2010).
31. Shakhova, N., Semiletov, I. & Chuvilin, E. Understanding the permafrost-hydrate system and associated methane releases in the East Siberian Arctic Shelf. *Geosciences* **9**, 251 (2019).
32. Archer, D. A model of the methane cycle, permafrost, and hydrology of the Siberian continental margin. *Biogeosciences* **12**, 2953–2974 (2015).
33. Sparrow, K. J. & Kessler, J. D. Comment on The origin of methane in the East Siberian Arctic Shelf unraveled with triple isotope analysis by Sapart *et al.* (2017). *Biogeosciences* **15**, 4777–4779 (2018).
34. Thornton, B. F. & Crill, P. Microbial lid on subsea methane. *Nat. Clim. Change* **5**, 723–724 (2015).
35. Sparrow, K. J. *et al.* Limited contribution of ancient methane to surface waters of the US Beaufort Sea shelf. *Sci. Adv.* **4**, 4842 (2018).
36. Steinbach, J. *et al.* Source apportionment of methane escaping the subsea permafrost system in the outer Eurasian Arctic Shelf. *Proc. Natl. Acad. Sci.* **118**, 2118 (2021).
37. Wild, B. *et al.* Organic matter composition and greenhouse gas production of thawing subsea permafrost in the Laptev Sea. *Nat. Commun.* **13**, 5057 (2022).
38. Ruppel, C. Permafrost-associated gas hydrate: Is it really approximately 1% of the global system? *J. Chem. Eng. Data* **60**, 429 (2015).
39. Hugelius, G. *et al.* Estimated stocks of circumpolar permafrost carbon with quantified uncertainty ranges and identified data gaps. *Biogeosciences* **11**, 6573–6593 (2014).
40. Hugelius, G. *et al.* Large stocks of peatland carbon and nitrogen are vulnerable to permafrost thaw. *Proc. Natl. Acad. Sci.* **117**, 20438–20446 (2020).
41. Mishra, U. *et al.* Spatial heterogeneity and environmental predictors of permafrost region soil organic carbon stocks. *Sci. Adv.* **7**, 5236 (2021).
42. Strauss, J. *et al.* *Recarbonizing Global Soils: A Technical Manual of Best Management Practices* (Food and agriculture Organization of the United Nations, 2021).
43. Strauss, J. *et al.* Deep Yedoma permafrost: A synthesis of depositional characteristics and carbon vulnerability. *Earth Sci. Rev.* **172**, 75–86 (2017).
44. Strauss, J. *et al.* The deep permafrost carbon pool of the Yedoma region in Siberia and Alaska. *Geophys. Res. Lett.* **40**, 6165–6170 (2013).
45. Obu, J. *et al.* Northern Hemisphere permafrost map based on TTOP modelling for 2000–2016 at 1 km² scale. *Earth Sci. Rev.* **193**, 299–316 (2019).
46. Tesi, T. *et al.* Massive remobilization of permafrost carbon during post-glacial warming. *Nat. Commun.* **7**, 13653 (2016).

47. Martens, J. *et al.* Remobilization of old permafrost carbon to Chukchi sea sediments during the end of the last deglaciation. *Glob. Biogeochem. Cycles* **33**, 2–14 (2019).
48. Martens, J. *et al.* Remobilization of dormant carbon from Siberian-Arctic permafrost during three past warming events. *Sci. Adv.* **6**, 6546 (2020).
49. Winterfeld, M. *et al.* Deglacial mobilization of pre-aged terrestrial carbon from degrading permafrost. *Nat. Commun.* **9**, 3666 (2018).
50. Strauss, J. *et al.* Circum-Arctic map of the Yedoma permafrost domain. *Front. Earth Sci.* **9**, 1001 (2021).
51. Gavrilov, A., Romanovskii, N. & Hubberten, H.-W. Paleogeographical scenario of late-glacial transgression on the Laptev Sea shelf. *Earth Cryosphere* **10**, 39–50 (2006).
52. Martens, J., Wild, B., Semiletov, I., Dudarev, O. V. & Gustafsson, Ö. Circum-Arctic release of terrestrial carbon varies between regions and sources. *Nat. Commun.* **13**, 5858 (2022).
53. Martens, J. *et al.* CASCADE—The circum-arctic sediment CARbon DatabasE. *Earth Syst. Sci. Data Discuss.* **2020**, 1–26 (2020).
54. Overduin, P. P. *et al.* Methane oxidation following submarine permafrost degradation: Measurements from a central Laptev Sea shelf borehole. *J. Geophys. Res. Biogeosci.* **120**, 965–978 (2015).
55. Winterfeld, M. *et al.* Coastal permafrost landscape development since the Late Pleistocene in the western Laptev Sea, Siberia. *Boreas* **40**, 697–713 (2011).
56. Waseda, A. & Uchida, T. Summary and implications of the Mallik 2002. In *Gas Hydrate Production Research Well Program, Mackenzie Delta, Northwest Territories* (eds Dallimore, S. R. & Collett, T. S.) 11 (Canada. Geological Survey of Canada, 2005).
57. Boudreau, B. P. & Ruddick, B. R. On a reactive continuum representation of organic matter diagenesis. *Am. J. Sci.* **29**, 507–538 (1991).
58. Arndt, S. *et al.* Quantifying the degradation of organic matter in marine sediments: A review and synthesis. *Earth Sci. Rev.* **123**, 53–86 (2013).
59. Freitas, F. S. *et al.* Benthic-pelagic coupling in the Barents Sea: An integrated data-model framework. *Philos. Trans. R. Soc. A Phys. Eng. Sci.* **378**, 2181 (2020).
60. Schirrmeister, L. *et al.* Fossil organic matter characteristics in permafrost deposits of the northeast Siberian Arctic. *J. Geophys. Res. Biogeosci.* **116**, 2 (2011).
61. Dmitrenko, I. A. *et al.* Recent changes in shelf hydrography in the Siberian Arctic: Potential for subsea permafrost instability. *J. Geophys. Res. Oceans* **116**, C10027 (2011).
62. Chuvilin, E., Grebenkin, S. & Zhmaev, M. Gas permeability of sandy sediments: Effects of phase changes in pore ice and gas hydrates. *Energy Fuels* **35**, 7874 (2021).
63. Walter Anthony, K., Anthony, P., Grosse, G. & Chanton, J. Geologic methane seeps along boundaries of Arctic permafrost thaw and melting glaciers. *Nat. Geosci.* **5**, 419–426 (2012).
64. Ruppel, C. & Kessler, J. D. The interaction of climate change and methane hydrates. *Rev. Geophys.* **55**, 126 (2017).
65. Chuvilin, E. & Bukhanov, B. Effect of hydrate formation conditions on thermal conductivity of gas-saturated sediments. *Energy Fuels* **31**, 5246–5254 (2017).
66. Sun, S., Gu, L., Yang, Z., Lin, H. & Li, Y. Thermophysical properties of natural gas hydrates: A review. *Nat. Gas Ind. B* **9**, 246–263 (2022).
67. Almenningen, S., Iden, E., Fernø, M. & Ersland, G. Salinity effects on pore-scale methane gas hydrate dissociation. *J. Geophys. Res. Solid Earth* **123**, 5599 (2018).
68. Paull, C. K. *et al.* Rapid seafloor changes associated with the degradation of Arctic submarine permafrost. *Proc. Natl. Acad. Sci.* **119**, e2119105119 (2022).
69. Frederick, J. & Buffett, B. Effects of submarine groundwater discharge on the present-day extent of relict submarine permafrost and gas hydrate stability on the Beaufort Sea continental shelf. *J. Geophys. Res. Earth Surf.* **120**, 417 (2015).
70. LaRowe, D. *et al.* The fate of organic carbon in marine sediments—New insights from recent data and analysis. *Earth Sci. Rev.* **204**, 103146 (2020).
71. Mostovaya, A., Hawkes, J. A., Koehler, B., Dittmar, T. & Tranvik, L. J. Emergence of the reactivity continuum of organic matter from kinetics of a multitude of individual molecular constituents. *Environ. Sci. Technol.* **51**, 11571–11579 (2017).
72. Schmidt, M. W. I. *et al.* Persistence of soil organic matter as an ecosystem property. *Nature* **478**, 49–56 (2011).
73. Wologo, E. *et al.* Stream dissolved organic matter in permafrost regions shows surprising compositional similarities but negative priming and nutrient effects. *Glob. Biogeochem. Cycles* **35**, e2020GB006719 (2021).
74. Mayer, L. M. Sedimentary organic matter preservation: An assessment and speculative synthesis—A comment. *Mar. Chem.* **49**, 123–126 (1995).
75. Middelburg, J. J. *Marine Carbon Biogeochemistry: A Primer for Earth System Scientists* 126 (Springer, 2019).
76. LaRowe, D. E. *et al.* Organic carbon and microbial activity in marine sediments on a global scale throughout the quaternary. *Geochim. Cosmochim. Acta* **286**, 227–247 (2020).
77. Westermann, S., Schuler, T. V., Gislén, K. & Eitzel, B. Transient thermal modeling of permafrost conditions in Southern Norway. *The Cryosphere* **7**, 719–739 (2013).
78. Straume, E. O. *et al.* GlobSed: Updated total sediment thickness in the world's oceans. *Geochem. Geophys. Geosyst.* **20**, 1756–1772 (2019).
79. Davies, J. H. Global map of solid Earth surface heat flow. *Geochem. Geophys. Geosyst.* **14**, 4608–4622 (2013).
80. Grant, K. M. *et al.* Sea-level variability over five glacial cycles. *Nat. Commun.* **5**, 9 (2014).
81. Ganopolski, A., Calov, R. & Claussen, M. Simulation of the Last Glacial cycle with a coupled climate ice-sheet model of intermediate complexity. *Clim. Past* **6**, 229–244 (2010).
82. Ganopolski, A. & Brovkin, V. Simulation of climate, ice sheets and CO₂ evolution during the last four glacial cycles with an Earth system model of intermediate complexity. *Clim. Past* **13**, 1695–1716 (2017).
83. Middelburg, J. J. A simple rate model for organic matter decomposition in marine sediments. *Geochim. Cosmochim. Acta* **53**, 1577–1581 (1989).
84. Westrich, J. T. & Berner, R. A. The role of sedimentary organic matter in bacterial sulfate reduction—The G model tested. *Limnol. Oceanogr.* **29**, 236–249 (1984).
85. Freitas, F. S. *et al.* New insights into large-scale trends of apparent organic matter reactivity in marine sediments and patterns of benthic carbon transformation. *Biogeosciences* **18**, 4651–4679 (2021).
86. Schädel, C. *et al.* Circumpolar assessment of permafrost C quality and its vulnerability over time using long-term incubation data. *Glob. Change Biol.* **20**, 641–652 (2014).
87. in 't Zandt, M. H., Liebner, S. & Welte, C. U. Roles of Thermokarst lakes in a warming world. *Trends Microbiol.* **28**, 769–779 (2020).
88. Overduin, P. P. *et al.* Submarine Permafrost Map (SuPerMAP), modeled with CryoGrid 2, Circum-Arctic. PANGAEA. <https://doi.org/10.1594/PANGAEA.910540> (2020).

Author contributions

Conceptualization by F.M., G.G., P.O., S.A., T.S.v.D. and V.B. Code development and resources were contributed by F.M., S.W., M.L., P.O., S.A. and T.S.v.D. J.S. provided validation. All authors contributed to all stages of writing the manuscript. Funding acquisition P.O. and S.W.

Funding

Open Access funding enabled and organized by Projekt DEAL. This publication is part of the Nunataryuk project. The project has received funding under the European Union's Horizon 2020 Research and Innovation Programme under Grant Agreement No. 773421. ML and TSvD were supported by a Grant of the Federal Ministry of Education and Research (BMBF) of Germany (No. 01LN1709A). This publication is supported by the Open Access Publication Funds of Alfred-Wegener-Institut Helmholtz-Zentrum für Polar- und Meeresforschung.

Competing interests

The authors declare no competing interests.

Additional information

Supplementary Information The online version contains supplementary material available at <https://doi.org/10.1038/s41598-023-36471-z>.

Correspondence and requests for materials should be addressed to F.M.

Reprints and permissions information is available at www.nature.com/reprints.

Publisher's note Springer Nature remains neutral with regard to jurisdictional claims in published maps and institutional affiliations.



Open Access This article is licensed under a Creative Commons Attribution 4.0 International License, which permits use, sharing, adaptation, distribution and reproduction in any medium or format, as long as you give appropriate credit to the original author(s) and the source, provide a link to the Creative Commons licence, and indicate if changes were made. The images or other third party material in this article are included in the article's Creative Commons licence, unless indicated otherwise in a credit line to the material. If material is not included in the article's Creative Commons licence and your intended use is not permitted by statutory regulation or exceeds the permitted use, you will need to obtain permission directly from the copyright holder. To view a copy of this licence, visit <http://creativecommons.org/licenses/by/4.0/>.

© The Author(s) 2023